

# 1 Integrated Geophysical Analysis of Rangpur Saddle: Insights on Tectonics and 2 Magnetic Mineral Potential of North-Western Bangladesh

3  
4 Mohammad Tawhidur Rahman Tushar<sup>1</sup>, Asif Ashraf<sup>2</sup>, Md. Mahfuz Alam<sup>1</sup>, Md Nasif Jamil<sup>1</sup>, Saba Karim<sup>1</sup>,  
5 Md. Shahjahan<sup>3</sup>, Md. Anwar Hossain Bhuiyan<sup>1</sup>

6  
7 <sup>1</sup>Department of Geology, University of Dhaka, Dhaka-1000, Bangladesh

8 <sup>2</sup>Department of Earth Sciences, University of Oregon, Eugene, Oregon-97401, United States of America

9 <sup>3</sup>Geological survey of Bangladesh, 153 Pioneer Road, Dhaka-1000, Bangladesh

10  
11 *Correspondence to: Mohammad Tawhidur Rahman Tushar (mtrt@du.ac.bd) and Asif Ashraf (aashraf@uoregon.edu)*

## 12 13 Abstract

14  
15 The northwestern region of Bangladesh holds untapped potential for magnetic mineral deposits at  
16 shallow depths. Unlike much of Bangladesh, characterized by thick sediments of the Bengal Basin,  
17 this area is an extension of the Indian Shield, often referred to as the Stable Platform. It is also  
18 geologically distinct, hosting structures related to the breakup of Pangea. The geology and  
19 tectonics of this region have remained largely understudied. To address this gap, this study  
20 integrates gravity, magnetic, seismic, and drilling data to investigate the subsurface structure and  
21 evaluate the resource potential of the area. We utilize advanced filtering and modeling techniques,  
22 including tilt derivatives and horizontal gradient methods, to understand the tectonic framework  
23 and geometry of the subsurface structures. Our spatial analysis, using multiple geophysical  
24 datasets, reveals dipolar magnetic anomalies, which we attribute to gabbroic intrusions along  
25 extensional faults that define the region's horst and graben structures. To validate our  
26 interpretations, we developed an integrated 2-D subsurface model that aligns with the observed  
27 geophysical data. However, the study is limited by the availability of high-resolution seismic data  
28 and the sparse distribution of drilling locations, which may affect the precision of our subsurface  
29 characterization. Our findings provide crucial insights into the tectonic evolution of the stable  
30 platform and underscore the economic potential of the Rangpur Saddle, the shallowest part of the  
31 stable platform, for mineral exploration. These insights pave the way for further exploration and  
32 development initiatives focused on uncovering the mineral wealth of this underexplored region.

## 33 34 1. Introduction

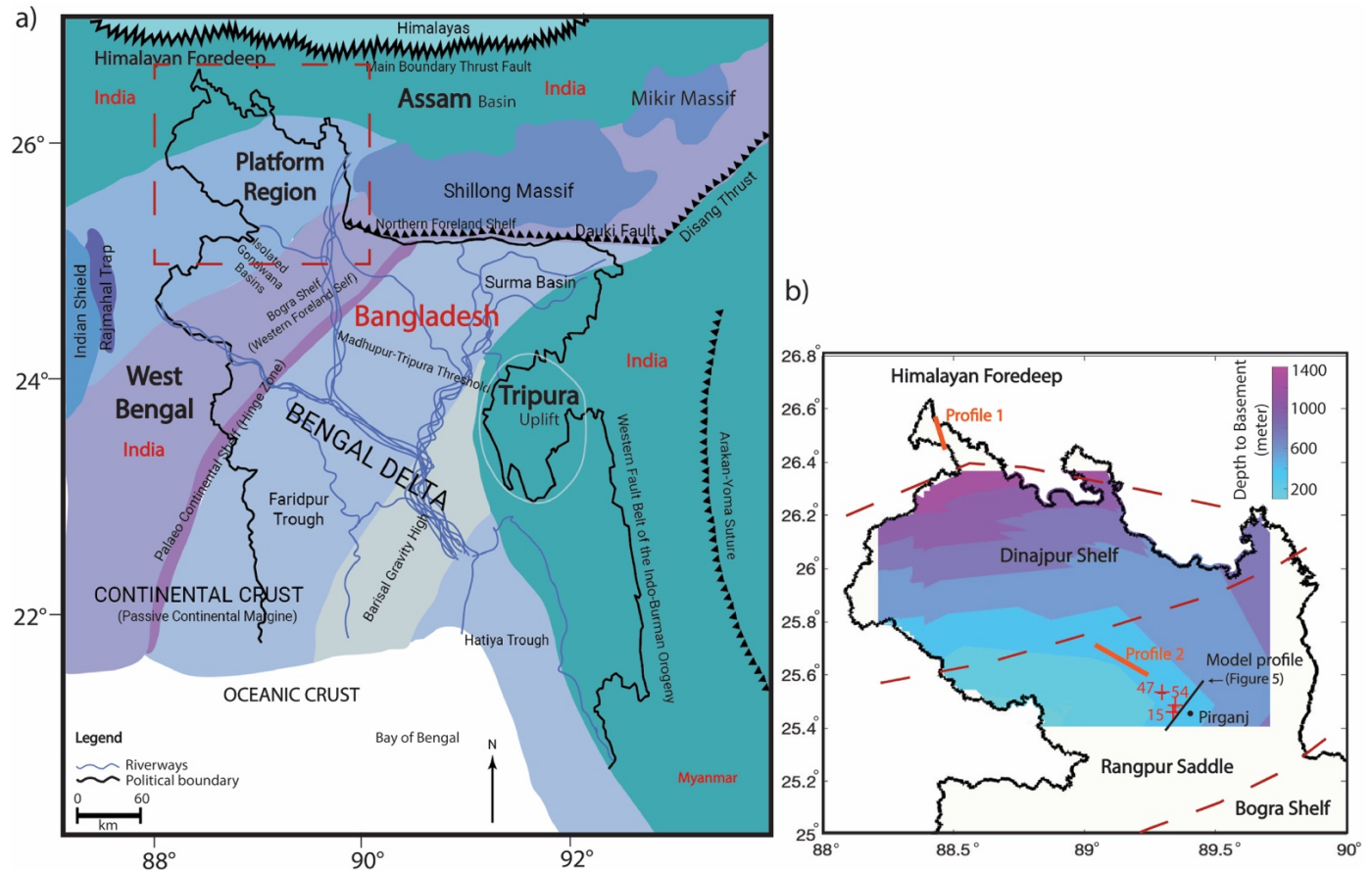
35  
36 The northwestern part of Bangladesh is rich in potential mineral resources. The geological  
37 diversity of this area suggests the presence of other valuable minerals that remain largely  
38 unexplored (Akhtar, 2005; Hasan et al., 2023; Moon, 2022). In this area, basement rocks are  
39 present at relatively shallow depths of 128 meters, hosting a spectrum of economic mineral  
40 resources, including coal, limestone, white clay, and hard rock (Khan and Rahman, 1992).  
41 Notably, Pirganj in the Rangpur district (**Figure 1**) records the country's highest magnetic  
42 anomaly, suggesting the potential for magnetic mineral ore deposits. In the 1990s, drilling  
43 activities were conducted in the region after developing a 2D subsurface model by the Geological  
44 Survey of Bangladesh (GSB) in collaboration with the United States Geological Survey (USGS).  
45 Despite these efforts, no noteworthy ore body was identified during the drilling process (Rahman

46 and Ullah, 2009). Moreover, the tectonic evolution of the Paleo-Proterozoic basement in the  
47 northwest region of the Bengal Basin still needs to be studied.

48  
49 The study area is located in a region commonly referred to as the Rangpur platform or saddle  
50 (Masum et al., 2021), an eastern extension of the Indian Shield (Alam et al., 2003). The northern  
51 part of the Rangpur Saddle rests on a shallow Precambrian basement, ranging from 130 to 1000  
52 meters in depth. This area of Bangladesh is geologically stable, characterized predominantly by  
53 horsts and grabens, which were formed during the Cretaceous rifting of the Indian plate from the  
54 Antarctica-Australia section of Gondwanaland (Curry, 1991; Curry and Moore, 1974). Although  
55 the basement primarily consists of diorite, tonalite, and granodiorite, it is also intersected by  
56 pegmatite and mafic/ultramafic dykes (Hossain et al., 2007; Kabir et al., 2001).

57  
58 In this study, we explore the possibility of mafic dykes as the source of high magnetic anomalies  
59 using multiple geophysical datasets while establishing the regional geological structure of this  
60 significantly understudied area. We aim to conduct integrated spatial analysis and develop  
61 subsurface models with gravity, magnetic, seismic, and drilling data to understand the regional  
62 geological features. Gravity and magnetic data are widely used to understand and characterize  
63 geological formations, particularly for identifying thin magnetic layers or faults (Adebiyi et al.,  
64 2023; Jaffal et al., 2010). High-resolution potential field data help identify structures related to  
65 local-scale mineralization that are covered by shallow alluvium or other unconsolidated sediments  
66 (Hendrickson, 2016; McCafferty et al., 2014). Since potential field data can yield multiple  
67 solutions (Filina et al., 2019), we also incorporate seismic and drilling data to constrain the  
68 subsurface framework and produce more reliable results (Sundararajan, 2012). Our study applies  
69 various filters to magnetic and gravity data to enhance and delineate regional crustal structures,  
70 with a focus on highlighting structure edges where metallic mineral deposits are likely to be found  
71 (Hildenbrand, 2000).

72



73  
 74 Figure 1: (a) Regional geological map of Bangladesh adopted from Hossain et al. (2019), illustrating various  
 75 geological and tectonic zones with distinct color coding. The names of neighboring countries are labeled in red. The  
 76 red dashed box indicates the study area in the northwestern part of Bangladesh. (b) The map of the northwestern  
 77 Bangladesh region shows basement depth with its tectonic subdivisions. Regional basement depths are collected from  
 78 GSB and constructed from various seismic reflection surveys. Red dashed lines mark the approximate boundaries of  
 79 the tectonic divisions. Seismic profiles (orange lines) and drilling locations (red plus signs) utilized in this study are  
 80 also highlighted. Our specific study area, Pirganj, is also shown on the map, where the highest magnetic anomaly is  
 81 observed. The integrated 2-D modeling profile of this study is also shown in this map with a solid black line.

82  
 83 **2. Geological setting**

84  
 85 Bangladesh, though geographically compact, possesses a complex and diverse geological  
 86 framework shaped largely by its position within the Bengal Basin (Roy and Chatterjee, 2015). This  
 87 region is primarily divided into two major tectonic units (Morgan and McIntire, 1959). To the  
 88 northwest of the hinge zone (see **Figure 1a** for location), the stable platform region features a  
 89 shallow basement composed predominantly of Precambrian-aged rocks (Uddin and Lundberg,  
 90 1998). Conversely, the southeastern portion of the Bengal Basin comprises a geosynclinal basin,  
 91 distinguished by significant sediment accumulation, with sediment thicknesses exceeding 12  
 92 kilometers (Alam, 1989). This tectonic configuration highlights the geological contrasts between  
 93 the stable platform and the more dynamic, subsiding basin to the southeast.

94  
 95 The Bengal Basin, encompassing Bangladesh and parts of the neighboring Indian states of West  
 96 Bengal, Assam, and Tripura, is situated at the northeastern edge of the Indian craton. It is one of

97 South Asia's largest peripheral collisional foreland basins, with a sedimentary sequence spanning  
98 from the Early Cretaceous to the Holocene (DeCelles, 2011). The study area, located in the  
99 northwest part of the basin and known as the stable platform, consists of three geological  
100 components (Hossain et al., 2019): the Dinajpur Shelf, Rangpur Saddle, and the Bogra Shelf  
101 (**Figure 1b**). The Himalayan Foredeep region, located just north of the Dinajpur Shelf, contains  
102 the deepest basement in the stable platform (**Figure 1b**) and hosts numerous faults associated with  
103 extensional tectonics (**Figure 2a**). South of the Foredeep region, the Dinajpur Shelf gently slopes  
104 northward toward the Himalayan Foredeep at an angle of 1-3 degrees and is covered by recent  
105 sedimentary deposits. The Rangpur Saddle, the southern block of the Dinajpur Shelf, connects the  
106 Indian Shield to the Shillong Plateau and contains the shallowest basement in the Bengal Basin  
107 (Jain et al., 2020) (**Figure 1b**). The Bogra Shelf, on the southern slope of the Rangpur Saddle, was  
108 formed during the Early Cretaceous rifting of the Indian plate from Gondwana (Alam, 1989; Alam  
109 et al., 2003). Both the Rangpur Saddle and Bogra Shelf host several horsts and graben, and half-  
110 graben basins (**Figure 2b**).

111  
112 The entire northwestern Bangladesh is geologically stable with minimal folding impact that can  
113 be traced back to Rodinia and Nuna or Columbia supercontinents (Ameen et al., 2007; Zhang et  
114 al., 2012). Ameen et al. (2007) suggest that the basement is a separate micro-continental fragment  
115 trapped during the northward migration of the Indian Plate, while Hossain et al. (2007) propose  
116 that it is a continuation of the central Indian tectonic zone. During the Precambrian, only the stable  
117 shelf of the Bengal basin was part of the Indian Plate within Gondwana. By the Middle Jurassic  
118 (~170–175 Ma), the Indian Plate began drifting and became isolated by the end of the Paleocene  
119 (~55.9 Ma) (Hossain et al., 2019). During the Late Paleozoic–Mid Mesozoic, the stable shelf was  
120 developed as an intra-cratonic rift basin with Gondwana sediments in graben structures, followed  
121 by Kerguelen igneous activity and widespread Rajmahal Trap volcanism (Hossain et al., 2019;  
122 Valdiya, 2016).

123  
124 The basement in our study area is the shallowest part of the Stable Shelf, which is uplifted to a  
125 depth of 128 m from the surface, overlain by the Plio-Pleistocene Dupi Tila Sandstone and  
126 Madhupur Clay, and is mainly composed of crystalline rocks, including granite, granodiorite, and  
127 gneiss (Alam et al., 2003; Hossain et al., 2007). There is no outcrop of Precambrian basement in  
128 this area, and the commonly observed horst and graben structures control the stratigraphic  
129 subdivision. The Precambrian basement in this region lies beneath thick Cenozoic clastic deposits  
130 and is primarily felsic in composition, intersected by mafic-ultramafic and occasional felsic dykes  
131 (Chowdhury et al., 2022). Fault-bound graben basins within the basement contain Carboniferous  
132 rock units from the Permian Period (286 to 245 million years ago) called the Gondwana formation,  
133 marking the oldest sedimentary rocks in Bangladesh (Alam et al., 2003; Jain et al., 2020). Above  
134 the Permian Gondwana formation is the Jurassic Rajmahal Trap Formation, consisting of volcanic  
135 basalt strata (Alam, 1989; Roy and Chatterjee, 2015). The Shibganj Trapwash Formation overlays  
136 it, formed through weathering and erosion of the underlying igneous rocks (Khan, 1991).

137  
138 The Rangpur Saddle serves as the subsurface extension of the Indian shield, stretching between  
139 the Shillong Plateau to the east and the Rajmahal Hills to the west. Geophysical studies have  
140 identified two major faults framing the Garo-Rajmahal gap: the Dhubri-Jamuna Fault (western  
141 edge of Garo Hills) and the Rajmahal Fault (eastern edge of Rajmahal Hills), which encloses the  
142 Rangpur saddle (Hossain et al., 2019). Tectonic activities, particularly extensional tectonics during

143 continental rifting, have significantly disrupted the basement topography, forming numerous  
 144 horsts and grabens (Ahamed et al., 2020; Khan and Rahman, 1992). Despite this, the study area  
 145 remains predominantly flat with sediment covers (Khan, 1991) from the Pleistocene to the  
 146 Holocene period (Reimann and Hiller, 1993). Near the Rangpur Saddle, the eastern part of the  
 147 Indian Shield includes three major tectonic domains: Singhbhum Craton, Singhbhum Mobile Belt,  
 148 and Chhotanagpur Gneissic Complex (Mukhopadhyay and Matin, 2020). Singhbhum Craton is  
 149 characterized by prolonged crustal evolution during the Archean, comprising lithologies such as  
 150 granitoids and metamorphic rocks. Singhbhum Mobile Belt underwent accretion and modification  
 151 through volcanics, dyke swarms, and various intrusive bodies in the Proterozoic. Chhotanagpur  
 152 Gneissic Complex comprises mainly of gneisses, amphibolites, and granulites with mafic dyke  
 153 swarms, forming a structurally complex mobile belt. The tectonics of this region can be  
 154 characterized by intra-cratonic structural depressions between the uplifted tectonic blocks. Seismic  
 155 reflection studies indicate that the Moho in this region is complex and laminated, suggesting a  
 156 history of tectonic and magmatic activity (Valdiya, 2016). In the West Bengal basin, the Moho is  
 157 relatively shallow and horizontal (at a depth of 36 km), while other nearby regions (e.g., Kutch  
 158 basin) have a dipping Moho influenced by tectonic processes (Rangin and Sibuet, 2017).

159  
 160 Magnetic minerals, particularly iron ore, are widely found across the Indian Shield. These iron  
 161 deposits typically appear as metamorphosed banded iron or silica formations. In eastern India, the  
 162 Precambrian iron ore of the Singhbhum-North Orissa region is a horseshoe-shaped synclinorium  
 163 that contains the most significant iron deposits near Bangladesh. The first discovery of iron ore in  
 164 Bangladesh is located on the Dinajpur slope of the Rangpur platform (Alam et al., 2003). Around  
 165 30 km southwest of our study area, Masum et al. (2021) report iron ore-bearing basement rock  
 166 about 30 km southwest of our study area, with the iron ores occurring as a thin, metamorphosed  
 167 laminated layer.

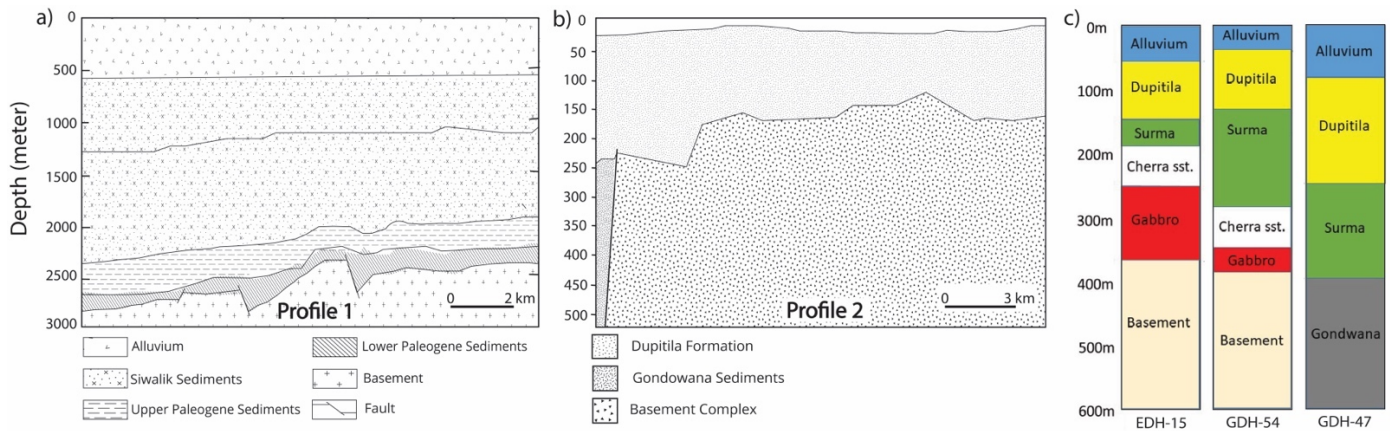
168  
 169 To understand the geological succession in Pirganj and its surroundings, we present a generalized  
 170 lithological depiction using data from EDH-15 and GDH-54 drill holes (Table 1).

171  
 172 Table 1: Stratigraphic Succession of Pirganj and its adjoining Areas according to drill holes EDH-15 and GDH-54  
 173

Age	Rock Units	Lithology	Thickness (m)
Recent	Alluvium	Loose sand, medium to coarse-grained	52
Unconformity			
Pliocene	Dupitila	Sandstone (SST), silty SST, pebbly SST, pebbly bed; SST: medium to coarse-grained, pebbles: quartzite, gneiss and schist	33
Unconformity			
Late Oligocene to Early Miocene	Surma	Alteration of SST and shales and their combination, sand and silty shale. SST: fine to medium-grained; shale: soft and sticky	125
Unconformity			

Late Cretaceous to Paleocene	Cherra Sandstone	Sandstone: medium to coarse-grained	50
Unconformity			
	Basement	Gabbro; Diorite, quartz diorite, granodiorite, quartz monazite.	180+ (base not seen)

174  
175



176  
177  
178  
179  
180  
181  
182

Figure 2: Interpretation of seismic and drilling data used for integrated geophysical analysis in this study. (a) and (b) present interpretations of the two seismic profiles analyzed. (c) shows the drilling log data, which correlates with the 2D subsurface models and assists in spatial analysis. Refer to Figure 1b for their locations. Seismic profile 1 is from Himalayan Foredeep region while profile 2 represents Rangpur Saddle. All the drilling logs are situated near the highest observed magnetic anomaly in Pirganj, located in Northwestern Bangladesh.

### 3. Data and Methodology

183  
184  
185  
186

#### 3.1 Geophysical Data

In this study, we apply an integrative analytical approach utilizing multiple geophysical datasets for spatial analysis and 2-D subsurface modeling. Our primary datasets are potential field data, specifically gravity and magnetic data, provided by the Geological Survey of Bangladesh (GSB). We use Bouguer gravity data and total magnetic intensity data for our analysis.

The gravity data presented in the paper were acquired through a land-based gravity survey conducted during the dry season (November–April) in the 1970s across approximately 8,000 km<sup>2</sup> in northwestern Bangladesh. Observation points were spaced 1–1.5 km apart, with elevations measured using digital leveling referenced to benchmarks from the Survey of Bangladesh. The Sylhet Gravity Base Station, connected to the IGSN 71 network, served as the national reference, and local sub-bases were established to correct for instrument drift. Two gravimeters were used—the analog Sodin Worden and the digital CG-5 AutoGrav with integrated GPS—with frequent cross-verification to ensure data accuracy. Standard geophysical corrections, including those for instrumental drift, tidal and latitude variations, and elevation differences, were applied, with Bouguer corrections calculated using a slab density of 2.0 g/cm<sup>3</sup>.

201  
202

203 Between 1979 and 1980, Hunting Geology & Geophysics Ltd. completed a nationwide  
204 aeromagnetic survey for the Government of Bangladesh, under the auspices of the Geological  
205 Survey of Bangladesh and Petrobangla. Flying a Geometrics G-803 proton magnetometer just 500  
206 ft ( $\approx 152$  m) above ground, the crew collected total-field data along flight lines oriented N  $45^\circ$  W  
207 on a nominal 3 km grid (locally tightened to 1 km) and crossed them with tie-lines oriented N  $45^\circ$   
208 E at 5 km spacing. Measurements were recorded every two seconds with a resolution of  $\pm 0.05$  nT,  
209 within a regional field that varied from 44 848 nT to 47 086 nT (inclinations  $28^\circ 30'$ – $38^\circ 30'$ ,  
210 declinations  $13^\circ$  W– $37^\circ$  W). All readings were archived in both digital and analogue form, and the  
211 data were uniformly shifted upward by 900 nT so that every value is positive.

212  
213 The topography data used in our geophysical modelling (**Figure S1**) are obtained from the online  
214 repository of the Scripps Institution of Oceanography, which are derived from satellite altimetry  
215 (Smith and Sandwell, 1997). Additionally, we incorporate interpretations of seismic images  
216 obtained from GSB to correlate our findings from gravity and magnetic data. However, raw  
217 seismic images are unavailable, as private entities originally collected them. To further refine our  
218 2-D integrated modeling, we use drilling data from three boreholes near our study area, also  
219 provided by GSB (see **Figure 1b** for the locations).

220

### 221 **3.2 Methods**

222  
223 For geophysical spatial analysis, we use gravity and magnetic anomaly maps. The Bouguer gravity  
224 data from GSB are corrected for elevation. For the total magnetic intensity map, we apply a  
225 differential reduction to the pole (RTP) to adjust the magnetic grid (Arkani-Hamed, 2007). This  
226 correction involves computing magnetic inclination, declination, and total magnetic field values  
227 based on the International Geomagnetic Reference Field (Alken et al., 2021) with a magnetic epoch  
228 of 1980.

229  
230 The next step in our spatial analysis methodology involves removing the regional trend from both  
231 the gravity and magnetic data. This process, known as regional-residual separation, is essential for  
232 isolating local anomalies by filtering out the broader, long-wavelength trends associated with  
233 large-scale geological structures (Ashraf and Filina, 2023b; Kheyrollahi et al., 2021; Núñez-  
234 Demarco et al., 2023). Total magnetic intensity anomalies arise from the combined effect of  
235 induced and remanent magnetization in rocks. Induced magnetization is caused by the Earth's  
236 ambient field acting on magnetic minerals, so it is aligned parallel to the present field, whereas  
237 remanent magnetization is a permanent magnetization inherent to the rocks (acquired in the past)  
238 that often points in a different direction (reflecting the Earth's field at the time of rock formation).  
239 The total magnetization is the vector sum of the induced and remanent contributions. As a result,  
240 the direction and relative magnitude of each component strongly influence the observed anomaly.  
241 If the induced and remanent magnetization vectors are aligned, they reinforce each other to  
242 produce a stronger (high-amplitude) anomaly; if they are opposed or significantly misaligned, they  
243 partially cancel or reorient the net magnetization, which can weaken the anomaly or even yield  
244 one of opposite polarity compared to what an induced-only model would predict. This interplay  
245 complicates data interpretation, since assuming all magnetization is induced (parallel to today's  
246 field) can lead to errors in locating or characterizing sources.

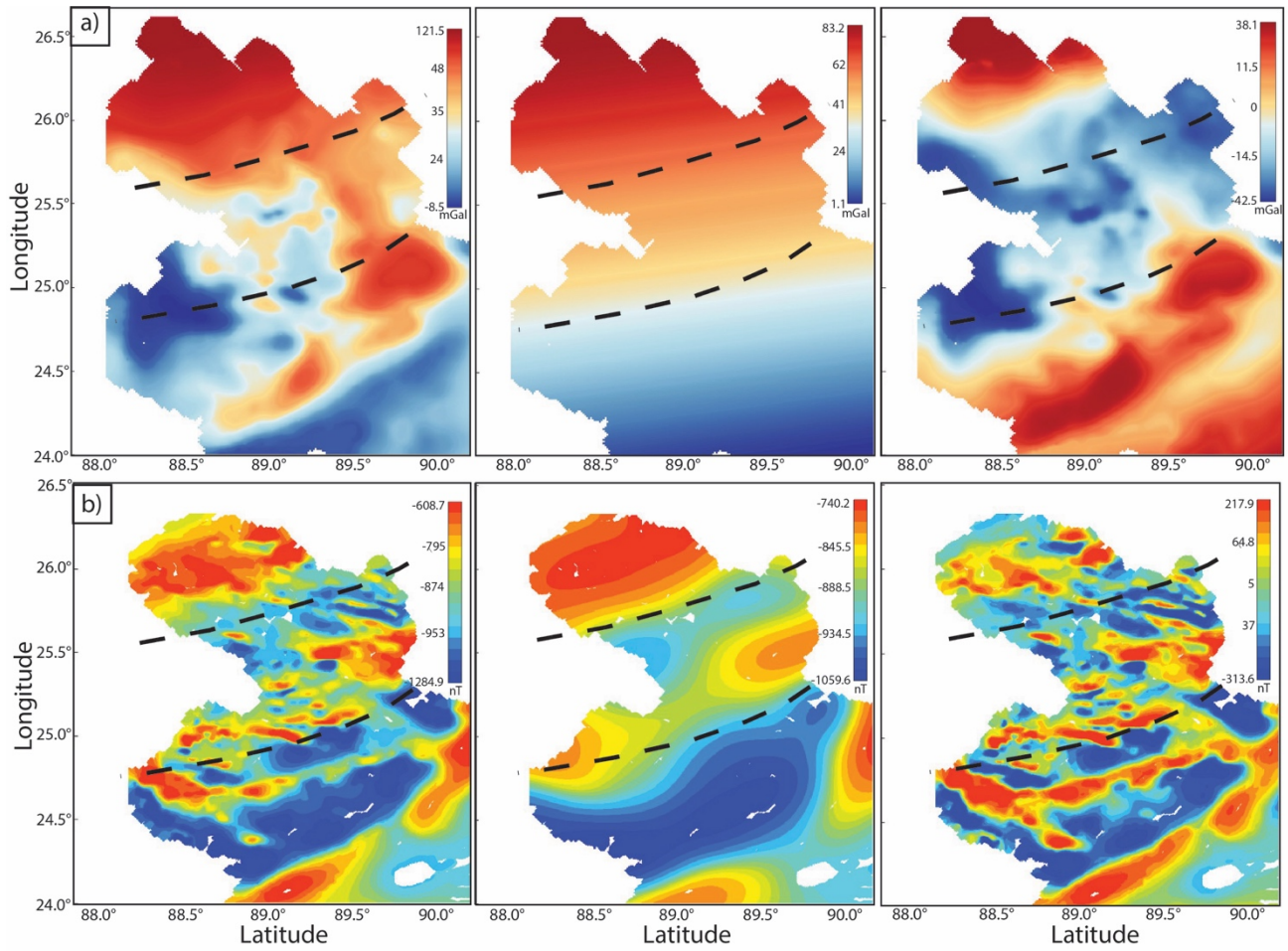
247  
248 By removing these regional trends, we enhance the visibility of smaller-scale or high-frequency  
249 anomalies, allowing subtle features and variations in the subsurface to be highlighted more

250 effectively. To remove regional anomalies, we apply an upward continuation of 1000 m to the  
251 Bouguer gravity data (**Figure 3a**). This approach simulates measuring the gravity field at a higher  
252 elevation—1000 m in our case—effectively smoothing out high-frequency anomalies associated  
253 with shallow or near-surface geological features (Balogun et al., 2023). For RTP magnetic  
254 anomaly, we use a Gaussian filter to calculate the regional trend (**Figure 3b**). This Gaussian filter  
255 acts as a low-pass filter, smoothing out high-frequency components in the dataset. After extracting  
256 the regional anomaly from the potential field, we subtract it from the unfiltered total anomaly,  
257 yielding the residual anomaly (**Figure 3**).

258  
259 We apply several filters to the residual potential field data to enhance specific features and improve  
260 interpretability (**Figure 3**). Under the framework of Poisson’s theorem in potential-field theory,  
261 taking a vertical derivative of gravity and performing a reduction-to-the-pole on magnetic data are  
262 mathematically analogous operations and are equivalent Fourier-domain operations: both sharpen  
263 source-edge contrasts while suppressing deep, long-wavelength signals, thus yielding mutually  
264 consistent structural imagery (Blakely, 1996). The filters we have used involve various forms of  
265 derivative operations, which help to highlight changes in the data that correspond to geological  
266 boundaries, faults, or other structural details (Ibraheem et al., 2023; Ma et al., 2016; Nasuti et al.,  
267 2019; Núñez-Demarco et al., 2023). For the residual RTP magnetic data, we apply and show two  
268 filters: the horizontal derivative and the tilt derivative. The horizontal derivative filter, applied in  
269 x-direction (i.e., across the longitudes) and y-direction (i.e., across the latitudes), accentuates  
270 lateral changes in the magnetic field, helping to reveal abrupt variations. The tilt derivative filter,  
271 however, is especially effective as an edge detector. It operates by combining both vertical and  
272 horizontal gradients, effectively highlighting the edges of anomalous bodies. The tilt derivative  
273 produces values that tend toward zero over magnetically flat regions, positive over rising areas,  
274 and negative over falling areas, creating a clear demarcation of the edges of magnetic sources. As  
275 a result, this filter enhances the boundaries of anomalies and helps pinpoint the locations and  
276 shapes of features with minimal distortion across varying depths (Ashraf and Filina, 2023b; Pham  
277 and Oliveira, 2023). We apply the lineament mapping techniques to map major structural  
278 boundaries from the filtered magnetic data (Ashraf and Filina, 2023a, 2023b; Ogah and Abubakar,  
279 2024; Zhang et al., 2024). Our approach focused on identifying gaps between magnetic stripes,  
280 changes in the stripe orientation, and a significant reduction in stripe width. We also calculate the  
281 analytical signals of the magnetic anomalies to highlight the areas with high magnetizing  
282 amplitude (Nabighian, 1972; Roest and Pilkington, 1993) that may illuminate magnetic mineral  
283 deposits (Mohamed et al., 2022). To calculate the analytical signal of the residual magnetic data,  
284 we first compute the horizontal and vertical derivatives of the magnetic field in the x, y, and z  
285 directions. The analytical signal was then derived by taking the square root of the sum of the  
286 squares of these derivatives, yielding a map that represents the amplitude of the magnetic field  
287 independent of direction and highlights the edges of magnetic sources. To validate our  
288 interpretations, we cross-reference the magnetic lineaments with gravity data. Before validating  
289 with gravity data, we filter the residual gravity data by applying the first vertical derivative and tilt  
290 derivative to map major tectonic structures and delineate their boundaries.

291  
292 We also develop 2-D integrated models of the subsurface to examine the variations in the physical  
293 properties of the rocks (density and magnetic susceptibility). We build our models using the GM-  
294 SYS module within the Geosoft software suite, employing a 2-D approximation (Geosoft, 2021).  
295 The GM-SYS model is extended to +/- 30000 km (i.e., infinity) along the X-axis and 90 km along

296 the Z-axis to eliminate edge effects. By integrating gravity and magnetic data within this 2D  
 297 context, we can delineate major geological boundaries and assess regional structural trends with  
 298 sufficient accuracy for our research objectives. Our goal is to develop a simple subsurface structure  
 299 that satisfactorily aligns with gravity, magnetic, and logging data without introducing excessive  
 300 complexity that might overfit the potential field anomaly. Instead, we aim to replicate the general  
 301 pattern of the observed anomaly in our 2D modeling, seeking to generate computed anomalies  
 302 with comparable amplitude, wavelength, and phase to those observed in the potential fields.  
 303



304  
 305  
 306 Figure 3: Potential field data maps of northwestern Bangladesh used in this study to analyze geological and tectonic  
 307 features. (a) Gravity anomaly maps: from left to right, the Bouguer gravity anomaly, regional Bouguer gravity anomaly  
 308 with 1000 m upward continuation, and residual Bouguer gravity anomaly. (b) Magnetic anomaly maps: from left to  
 309 right, the RTP total magnetic anomaly, regional magnetic anomaly after Gaussian filtering, and residual magnetic  
 310 anomaly. The black dashed lines show the boundary of Rangpur Saddle.  
 311

## 312 4. Result

### 313 4.1 Integrated spatial analysis

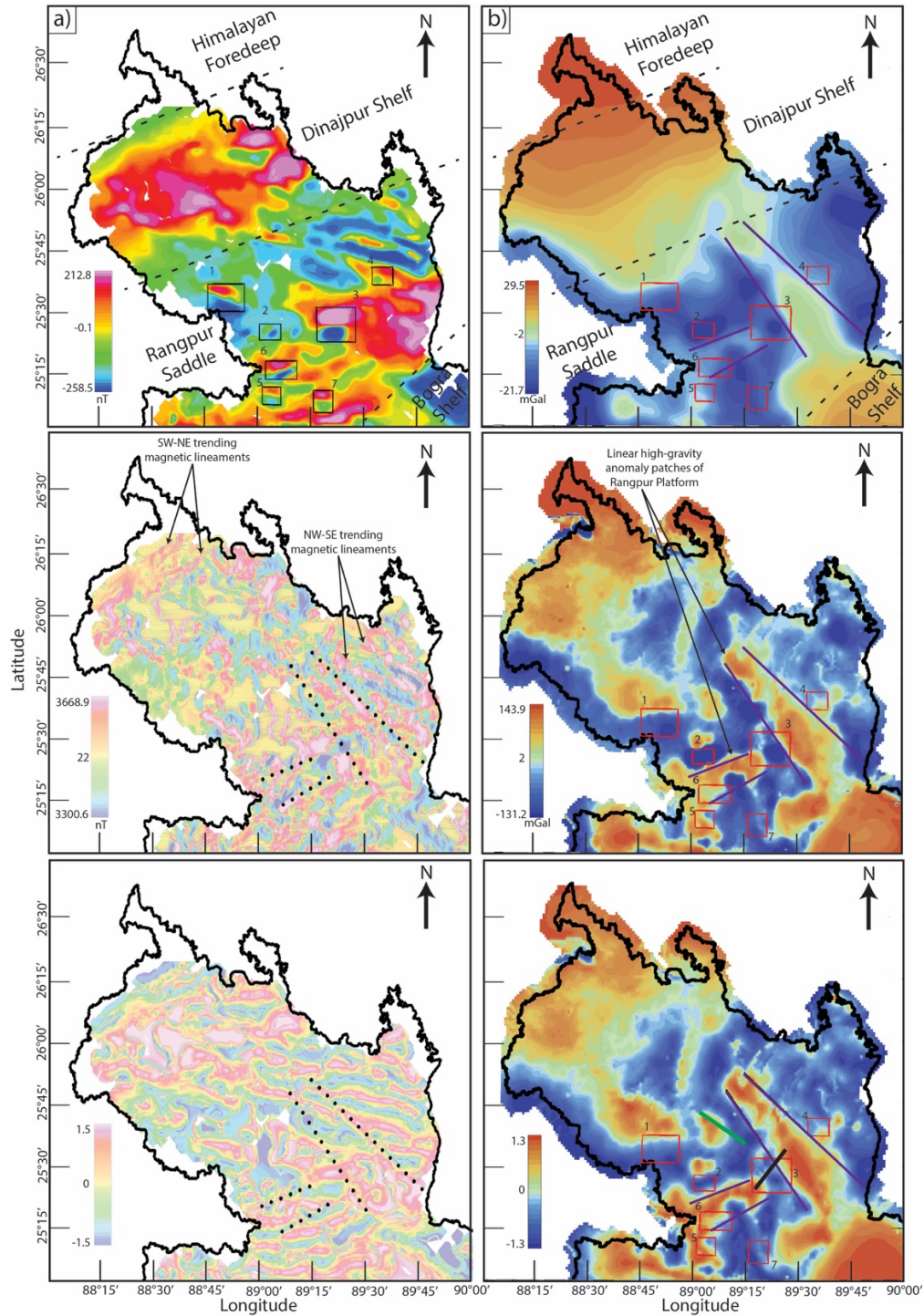
314  
 315  
 316 In this study, we first establish the regional tectonic structures of northwestern Bangladesh through  
 317 spatial analysis of multiple geophysical datasets. We utilize gravity, magnetic, seismic image

318 interpretations, and drilling log data to characterize the tectonic setup of this region. Our analysis  
319 of residual magnetic and gravity anomalies reveals that the Rangpur Saddle exhibits distinctly  
320 different geophysical characteristics compared to its northern counterpart, the Himalayan Foredeep  
321 region. These differences are discernible in the long-wavelength or broad-scale geophysical  
322 signatures across the two regions.

323  
324 In the Himalayan Foredeep, north of 26°N latitude, we observe a high residual Bouguer gravity  
325 anomaly, ranging from approximately 5 to 30 mGal. In contrast, the Rangpur Saddle, located south  
326 of this latitude, is marked by a low residual Bouguer gravity anomaly, typically between -22 and  
327 0 mGal. Similarly, the Rangpur Saddle shows lower residual RTP total magnetic anomalies,  
328 ranging from 0 to 260 nT compared to mostly high magnetic anomalies in north (~ 0 to 215 nT).  
329 The spatial patterns of these anomalies also differ across the regions. South of 26°N latitude, in  
330 the Rangpur Saddle, the horizontal and tilt derivative magnetic anomalies show a predominance  
331 of NW-SE trending magnetic lineaments. North of this latitude, in the Himalayan Foredeep, the  
332 magnetic anomaly trend shifts predominantly to a SW-NE orientation. Additionally, in the vertical  
333 and tilt derivatives of the gravity data, we observe the most pronounced high gravity linear  
334 anomaly patch trends NW-SE south of 26°N latitude, consistent with the magnetic anomaly trend  
335 in this area. South of 26°30'N latitude, we see another linear high-gravity patch in the filtered  
336 Bouguer gravity data trending NW-SE, indicating a different orientation than the other high-  
337 gravity patch of the Rangpur Saddle region. These two high-gravity patches are also traceable in  
338 the filtered magnetic anomalies, following the magnetic lineament mapping procedure. Notably,  
339 some areas exhibit strong inverse gravity and magnetic field trends, where high gravity coincides  
340 with low magnetic anomalies, or vice versa. One might expect a corresponding increase in the  
341 gravity signal due to the higher density of the gabbroic intrusions relative to the overlying rocks;  
342 however, this expected gravity anomaly is not observed in our data. We believe this discrepancy  
343 arises from two interconnected factors. First, gravity and magnetic methods are most sensitive to  
344 lateral variations in subsurface properties, and in our study area, the subsurface structures are  
345 predominantly flat-lying. At depth, the gabbroic intrusions are laterally adjacent to felsic basement  
346 rocks, and while the density contrast between these lithologies is modest (~0.1 g/cm<sup>3</sup>), their  
347 magnetic susceptibilities differ significantly. This contrast produces a strong magnetic response  
348 but only a subtle gravity anomaly that may be indistinguishable from background variations. Also,  
349 the intrusions occur in fault-bounded graben fill that causes a localized low density (due to thick  
350 low-density Gondwana sediments in the graben). Second, the spatial resolution of our gravity  
351 survey, with a station spacing of approximately 3 km, is relatively coarse compared to the scale of  
352 the gabbroic intrusions. As a result, any high-frequency gravity signals associated with these  
353 smaller or more localized bodies are likely undersampled and thus not adequately captured in the  
354 final gravity dataset. In brief, the high gravity areas correspond to uplifted blocks of dense  
355 basement, whereas the magnetic highs occur on the flanks where intrusions have come up along  
356 faults and the graben is filled with lighter sediment, yielding a relative gravity low.

357  
358 Within the Rangpur Saddle region, we observe multiple oval dipolar patterns. From the RTP  
359 residual magnetic anomaly data, we identify seven distinct patterns. The identification of these  
360 patterns follows several consistent criteria. First, the dipolar magnetic anomalies are generally  
361 oriented in a north-south direction. Second, each pattern features a magnetic high in the northern  
362 section and a corresponding low to the south. Third, within each pattern, the size, area, and  
363 amplitude of the magnetic high and low anomalies are comparable, contributing to a symmetrical

364 structure. The filtered magnetic data also reveals possible signatures of remanently magnetized  
365 sources, some of which may be reversely magnetized. At the Earth's magnetic field inclination of  
366 approximately  $45^\circ$  in northwestern Bangladesh (based on the IGRF 1980 epoch used for RTP  
367 correction), reversely magnetized sources such as gabbroic intrusions formed during past  
368 geomagnetic reversals produce negative anomalies after RTP where positive anomalies would  
369 align with the current field. Mapping these magnetic patterns onto the filtered gravity maps reveals  
370 that they consistently lie near the boundary between high and low gravity anomalies. While most  
371 of these magnetic patterns (patterns 1, 4, 5, 6, and 7) intersect only one boundary, a few patterns  
372 (specifically patterns 2 and 3) touch boundaries on both sides.  
373



374  
 375 Figure 4: a) Magnetic anomaly maps of northwestern Bangladesh. The top panel displays the residual RTP total  
 376 magnetic anomaly, the middle panel shows the first horizontal derivative in the x-direction (across longitudes), and  
 377 the bottom panel illustrates the tilt derivative. Black boxes highlight areas where oval dipolar magnetic patterns are  
 378 observed. Dotted black lines in the middle and bottom panels indicate boundaries of high gravity regions. b) Bouguer  
 379 gravity anomaly maps of northwestern Bangladesh. The top panel presents the residual Bouguer gravity anomaly, the  
 380 middle panel shows the first vertical derivative, and the bottom panel displays the tilt derivative. High gravity regions  
 381 are outlined by purple solid lines, and red boxes indicate areas with dipolar magnetic patterns. The solid green line in  
 382 the bottom panel represents seismic profile 2 from Figure 2. The thick solid black line shows the 2-D integrated  
 383 modelling profile of Figure 5.

## 4.2 Integrated subsurface modeling

We develop a 2-D subsurface model utilizing gravity, magnetic, and drilling log data (**Figure 5**). The goal of this model is to approximate the observed anomalies on a local scale while aligning with the available drilling log information (**Figure 2c**). The magnetic anomaly modeled in **Figure 5** is the residual RTP anomaly, reflecting local high-frequency features after removing regional trends. Importantly, we do not aim to achieve a precise fit between the observed data and calculated anomalies. This decision is driven by the fact that the observed potential field data are influenced by regional structures, and without sufficient seismic information, constructing a reliable regional model is not feasible. Instead, we focus on developing a simplified version of the subsurface model that reasonably fits the observed anomalies and drilling data.

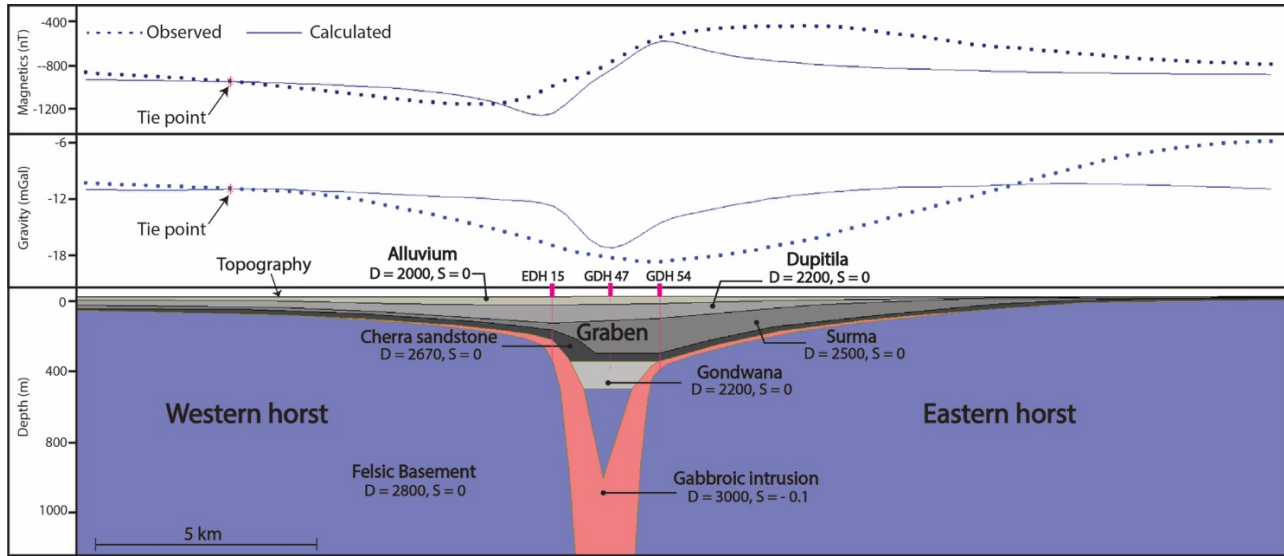
To ground the 2-D model in reality, we incorporated available drilling log information (**Figure 2**). Based on these logs, the model includes five sedimentary layers above a crystalline basement. The shallowest layer is assigned as alluvium, extending to a depth of 50 meters or less. Beneath the alluvium, we sequentially include the Dupitila, Surma, and Cherra sandstone layers. The variable thickness of these sedimentary layers comes from the drilling log information, except for the Gondwana layer. The thickness of Gondwana is approximated based on the gravity fit. Below these layers, we model a mafic intrusion of gabbro, which occurs within fault structures that have developed within the underlying felsic basement.

The resulting model indicates that a horst and graben structure is the most plausible configuration when considering the regional geological context. This structural interpretation also provides a reasonable match to the observed geophysical anomalies. Additionally, based on information from drilling log GDH 47, we assign a layer of Gondwana sediments within the graben basin, which is contributing to the low observed gravity in this region.

Densities in the model are derived from drilling data, reflecting the unique lithological characteristics of each unit. To get an initial guess on the density, we developed a gravity model for profile 1 that has seismic-derived subsurface information (**Figure S2**). The alluvium, Dupitila, Surma, and Cherra Sandstone layers are modeled with densities of 2000, 2200, 2500, and 2670 g/cm<sup>3</sup>, capturing their progressive compaction and mineral composition. The Gondwana unit, enriched with coal deposits, exhibits a notably lower density of 2200 g/cm<sup>3</sup>, consistent with its organic-rich composition. Beneath these layers, the felsic basement and gabbroic intrusion stand out with densities of 2800 and 3000 g/cm<sup>3</sup>, highlighting their denser crystalline structure and mafic origins.

Between 400 and 800 meters depth, the gabbroic intrusion begins to follow the fault plane. The thickness of both the Gondwana layer and the underlying felsic basement is determined from the amplitude of the calculated gravity and magnetic anomalies. The thickness of the Gondwana layer influences the minimum value of the calculated gravity anomaly, while the amplitude of the magnetic anomaly helps determine the depth of the gabbroic intrusion. Notably, our calculated anomalies are of high frequency. This occurs because our modeling does not incorporate all regional structures; instead, it focuses only on local structures. As a result, the calculated anomalies reflect primarily local or high-frequency potential field anomalies.

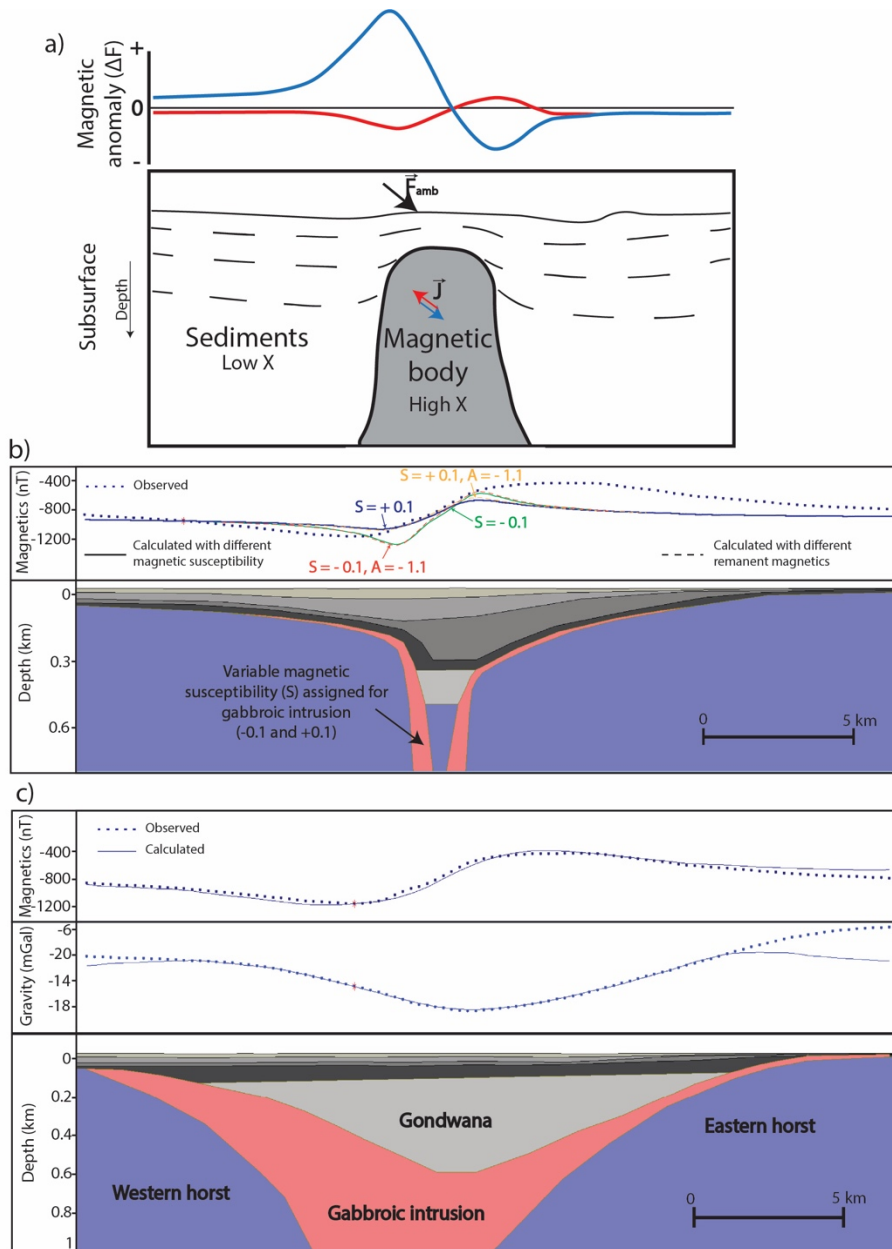
430 Our 2D subsurface model reveals two horst structures with a graben basin in the middle. We refer  
 431 to these as the eastern and western horsts based on their geographic locations. In the model, the  
 432 western horst structure is depicted as deeper, consistent with the observed gravity anomaly, which  
 433 shows lower gravity in the western horst compared to the eastern horst. Our model does not include  
 434 the broader horst structure on the eastern side, which likely explains the discrepancy between the  
 435 calculated and observed anomalies over the eastern horst.  
 436



437  
 438  
 439 Figure 5: Integrated 2D geophysical model over the highest magnetic anomaly in northwestern Bangladesh. See Figure  
 440 1b and 4c for the location of the model profile. The top panel presents the total magnetic intensity anomaly, and the  
 441 middle panel shows the gravity anomaly, with observed (dotted) and calculated (solid) data. Tie points, marked by red  
 442 stars, indicate where the calculated anomalies are vertically shifted to align with the observed data. The bottom panel  
 443 illustrates the subsurface model, with geological units represented by distinct colors. 'D' denotes density ( $g/cm^3$ ), and  
 444 'S' denotes magnetic susceptibility (SI units). Bold pink vertical dashes mark the locations of drilling logs used to  
 445 constrain subsurface units. Thin vertical pink lines extend downward from these surface locations. Solid pink lines  
 446 beneath EDH 15 and GDH 54 indicate where the forward model is directly tied to lithological boundaries from well  
 447 logs. In contrast, the dashed pink line beneath GDH 47 reflects an interpretative connection, as this well does not lie  
 448 directly along the modeling profile.  
 449

450 We acknowledge the mismatch between the observed and calculated anomalies in our forward  
 451 model. We aim to adopt the simplest model that captures the essential features of the observed  
 452 anomaly without introducing unnecessary complexity. While even basic 2-D models can yield  
 453 multiple valid solutions, incorporating intricate structures without strong geological constraints  
 454 would increase interpretive ambiguity. Additionally, our model is inherently two-dimensional and  
 455 thus cannot fully represent the three-dimensional geological variations present in the study area,  
 456 such as the broad, shallow eastern horst, whose lateral extent likely contributes to higher observed  
 457 gravity values. Finally, our modeling profile spans a smaller area than the full potential field survey  
 458 (refer to section 3.1), resulting in calculated anomalies that emphasize localized, high-frequency  
 459 features, whereas the observed data reflect broader, lower-frequency trends. Our forward model is  
 460 calculated on 250 m spacing, whereas the gravity data were acquired every 1–1.5 km and the  
 461 magnetic data every 5 km.  
 462

463 Furthermore, we also test alternative models, which further support that the presented version  
464 offers the most concise and geologically reasonable solution. First, we test how the polarization  
465 direction of the remanent magnetization affects the total magnetic intensity reading of a dome-  
466 shaped magnetic body (**Figure 6a**). We incorporate both remanent magnetization (A) and  
467 magnetic susceptibility (S) in the forward model affects the total magnetic intensity and its polarity  
468 (**Figure 6b**). When we assign a positive susceptibility contrast ( $S = +0.1$  SI), the calculated  
469 anomaly captures the general shape of the observed data more accurately in terms of slope, but the  
470 amplitude (highs and lows) is notably lower than the observed values. In contrast, using a negative  
471 susceptibility yields calculated amplitudes that closely match the observed highs and lows;  
472 however, the overall shape shows a poorer fit, with significant mismatches in the slopes. Because  
473 of the better match for the amplitudes, we prefer the negative susceptibility for the magnetic body  
474 in our forward model. We also implemented an additional component of remanent magnetization  
475 (A) to the magnetic body, fixed at  $-1.1$  A/m, and tested combinations such as  $S = -0.1$  SI with  $A$   
476  $= -0.1$  A/m and  $S = +0.1$  SI with  $A = -1.1$  A/m. These combinations yielded a similar response,  
477 primarily increasing the amplitude of the anomaly without changing the overall trend. In  
478 conclusion, while the additional remanent magnetization component amplifies the anomaly  
479 magnitude, it does not significantly affect the trend or alter the interpretation of the model. We  
480 have also developed a model that shows a perfect fit between the observed and calculated anomaly  
481 (**Figure 6c**). However, to achieve that, we need to completely abandon the constraints from well-  
482 logs and regional structural context based on gravity and magnetic data. For these reasons, we  
483 adopt a simplified, geologically grounded model that balances interpretive clarity with structural  
484 realism.  
485



486  
 487  
 488  
 489  
 490  
 491  
 492  
 493  
 494  
 495  
 496  
 497  
 498  
 499  
 500

Figure 6: a) Conceptual illustration showing polarization direction of the remanent magnetization affecting the total magnetic intensity reading of a dome-shaped magnetic body. The synthetic total-field anomaly ( $\Delta F$ ) profiles are calculated for a concealed high-susceptibility intrusion beneath low-susceptibility sediments. The blue curve represents the response when magnetization is purely induced parallel to the present-day ambient field  $F_{amb}$ , producing a simple positive-negative (dipolar) signature. The red curve shows how the anomaly shape and amplitude are modified when an oblique remanent magnetization component  $J$  is added to the induced vector. b) Investigation on how incorporating both remanent magnetization ( $A$ ) and magnetic susceptibility ( $S$ ) in the forward model affects the total magnetic intensity and its polarity. c) 2-D forward modelling along the same profile as Figure 5, where we have achieved a perfect fit between the calculated and observed anomalies except for the model edges.

## 5. Discussion

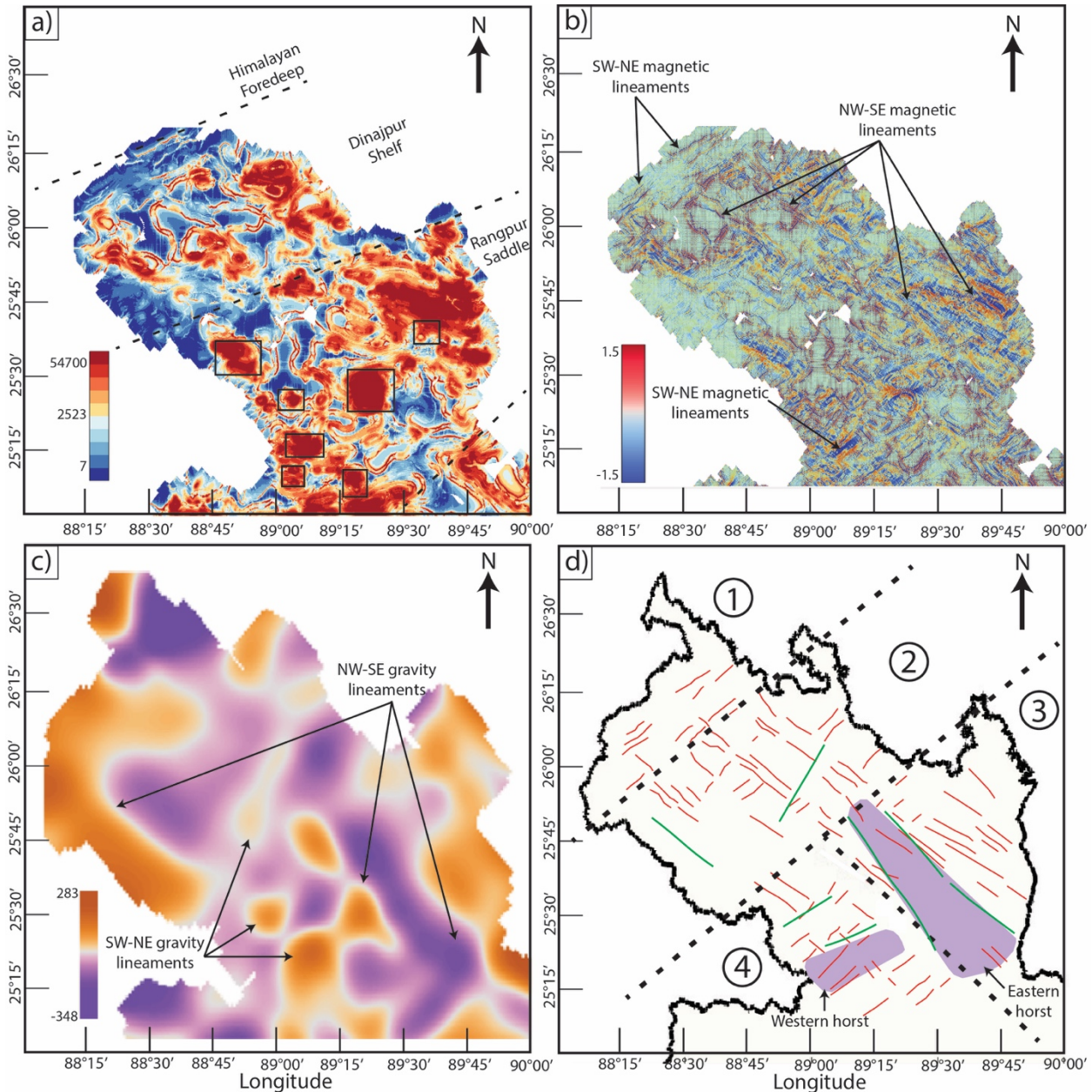
### 5.1 Basement structure

One of the primary goals of this paper is to understand the basement structure and tectonic setup of the Rangpur Saddle. Our findings reveal significant differences in the basement structures of the Rangpur Saddle compared to its northern counterparts, evident in both gravity and magnetic data. A key distinction is the depth to basement between these regions (**Figure 1b**). Previous studies consistently suggest that the basement depth in the Rangpur Saddle is shallower than in the Dinajpur Shelf. However, those studies were based on limited seismic and drilling data. Our results, however, indicate a more complex basement geometry than previously understood. Filtered gravity and seismic data presented here suggest that the Rangpur Saddle region contains both shallow and deep basement features (**Figure 4b**). Considering regional tectonics, we propose that high gravity values correspond to shallow horst structures, while low gravity values indicate deeper graben structures. However, the frequency of horsts and grabens is significantly lower in the Rangpur Saddle compared to the northern Himalayan Foredeep and the Dinajpur Shelf (**Figure 2a** and **2b**). In the Rangpur region, we identified only two horsts of notable width and length. The boundaries of these horst structures also appear as lineaments in the filtered magnetic data (**Figure 4a**), suggesting the presence of major structural boundaries.

Furthermore, differences in the directions of magnetic lineaments between the Rangpur Saddle region and its northern counterparts—the Dinajpur Shelf and the Himalayan Foredeep—suggest variations in paleo-tectonic stress orientation (**Figure 4a, 7a** and **7b**). Existing literature characterizes northwestern Bangladesh predominantly with extensional tectonics (Gani and Alam, 2003). Near the Himalayan Foredeep boundary, SW-NE trending magnetic lineaments indicate a paleo-principal stress direction oriented NW-SE. Moving southward into the Dinajpur Shelf, NW-SE trending magnetic lineaments become more common (**Figure 7b**), pointing to a shift in the principal stress direction associated with extensional tectonics. In the Rangpur Saddle, these NW-SE trending lineaments are even more frequent, especially in the eastern part, indicating a greater intensity of paleo-tectonic stress in this region compared to the Dinajpur Shelf. Based on traced magnetic and gravity lineaments, the stable platform can be divided into four distinct zones (**Figure 7d**). In Zone 1, located in the northern part, lineaments predominantly trend SW-NE, with only a few exceptions. Moving southward into Zone 2, there is a mixture of two differently trending lineaments: SW-NE and NW-SE. In Zone 3, in the easternmost section of the stable platform, lineaments primarily trend NW-SE, aligning with the eastern horst. Finally, in Zone 4, the southernmost region, lineaments generally follow an SW-NE trend, corresponding with the western horst. This subdivision highlights the complex nature of past tectonic processes in this region.

We also identify seven oval dipolar patterns of magnetic highs and lows. When mapped onto gravity data, these patterns consistently align with the boundaries between high and low gravity patches, indicating the possible boundaries between horsts and grabens. Drilling log data near the most prominent magnetic anomaly reveals the presence of gabbro, which may explain these dipolar magnetic patterns. Furthermore, these regions of dipolar magnetic patterns also spatially correlate with overall high magnetization (**Figure 7a**). We propose that these gabbro formations

546 resulted from intrusions along normal faults, formed by extensional tectonics, which define the  
 547 boundaries between horsts and grabens.  
 548



549  
 550 Figure 7: Filtered potential field maps of the northwestern stable platform region of Bangladesh, highlighting major  
 551 tectonic structures and boundaries. (a) Analytical signal map derived from the magnetic anomaly (methodology  
 552 detailed in Sect. 3), showing magnetization amplitudes across the region. Black boxes indicate areas of oval dipolar  
 553 magnetic patterns, as shown in Figure 4a. Dashed lines represent boundaries between established tectonic  
 554 subdivisions. (b) Total horizontal gradient map of the magnetic anomaly, calculated by applying a first horizontal  
 555 derivative filter in the X-direction, followed by a first horizontal derivative filter in the Y-direction. (c) Total horizontal  
 556 derivative (similar method as in 'b') of the residual gravity anomaly. This map is developed after applying upward  
 557 continuation to the residual gravity data to a level where high-resolution artifacts are no longer present in the derivative  
 558 map. (d) Map displaying traced magnetic lineaments (in red) from 'b' and gravity lineaments (in green) from 'c'.  
 559 Black dashed lines indicate regional subdivisions based on mapped tectonic lineaments. Purple polygons mark horst  
 560 structures in the Rangpur Saddle, interpreted from filtered gravity data (refer to Figure 4b).

561  
562  
563  
564  
565  
566  
567  
568  
569  
570  
571  
572  
573  
574  
575  
576  
577  
578  
579  
580  
581  
582  
583  
584  
585  
586  
587  
588  
589  
590  
591  
592  
593  
594  
595  
596  
597  
598  
599  
600  
601  
602  
603  
604  
605

## 5.2 Economic mineral potential

Our integrated spatial analysis and 2-D modeling reveal that the Rangpur Saddle contains at least two prominent horst and graben structures. The 2-D model results (**Figure 5**), supported by drilling log data, confirm the presence of gabbroic bodies along normal faults within these structures. This suggests that the most prominent oval-shaped dipolar magnetic signature has strong potential to host iron-bearing rocks such as gabbro. When the other similar patterns are mapped onto the gravity data, they consistently correspond to the boundaries between high and low gravity zones, marking the transitions between horsts and grabens. We interpret these gabbroic intrusions as products of magmatic emplacement along extensional faults (**Figure 8**), consistent with processes associated with the early stages of continental rifting. Furthermore, analysis of lineament orientations (**Figure 7d**) indicates that, except in the western horst region, most of the interpreted magmatic emplacement appears to be controlled by NW–SE oriented lineaments.

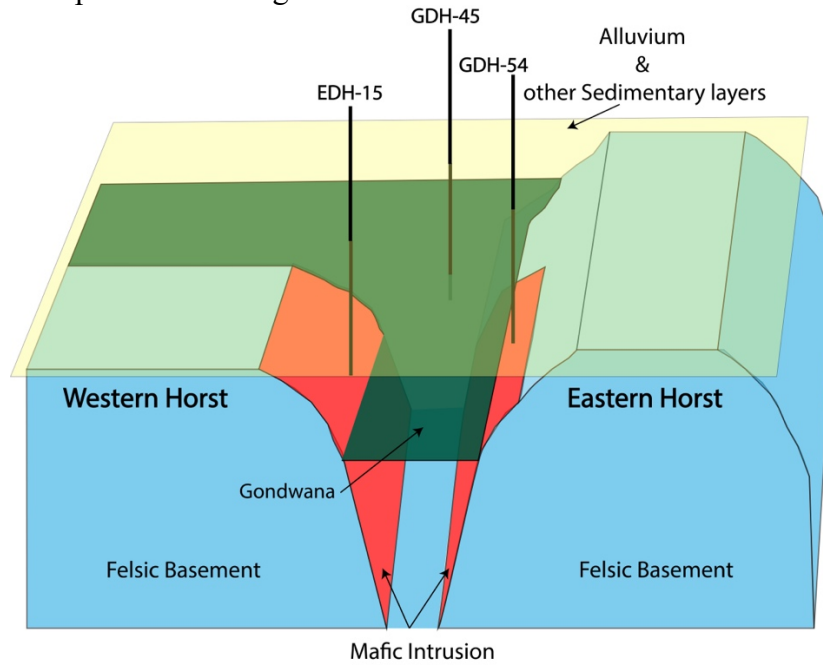
The breakup process involved rifting events that progressively separated the Indian subcontinent from the other Gondwanaland constituents (Veevers, 2004). The breakup of Gondwanaland involved multiple rifting episodes and magmatic activities. While the Central Atlantic Magmatic Province (CAMP) exemplifies rift-related magmatism during the Triassic-Jurassic breakup of Pangea, the Rangpur Saddle's tectonic evolution is more directly tied to the Cretaceous rifting of the Indian plate from Antarctica-Australia (Curry, 1991; Hossain et al., 2019). This rifting facilitated extensional faulting and mafic intrusions, analogous to processes observed in CAMP but occurring later in the Mesozoic. In such tectonic settings, normal faulting and rift-related subsidence create pathways for mafic magmas to ascend (Brune et al., 2023; Pirajno and Santosh, 2014; Ruppel, 1995), leading to the emplacement of gabbroic and other mafic intrusions within the crust (Magee et al., 2019).

Mafic magma intrusions are commonly observed along extensional fault planes in tectonically active regions worldwide. Troll et al. (2021) shows that in NW Scotland, Long Loch Fault acted as dynamic magma conduit with its movements facilitating the ascent of ultrabasic magmas. These magmas intruded along faults and fractures, leading to the destabilization and collapse of existing cumulate layers, forming extensive breccias. A study on Mesozoic gabbroic intrusions in the High Atlas Mountains highlights their emplacement along extensional faults during the rifting associated with the Central Atlantic Magmatic Province, where more than 50% of gabbro samples exhibit stable magnetization from magnetite which is identified as the primary component (Calvín et al., 2017). Fuller and Waters (1929) have extensively studied horsts and graben structures in southern Oregon where they found emplacement of volcanic and intrusive rocks are closely associated with extensional faulting. These normal faults and the resulting grabens provide pathways for magma to ascend and intrude, which is evident from the prevalence of rhyolitic, dacitic, and andesitic vents as well as basaltic dikes aligned with the faults.

Mafic intrusions along fault zones are often associated with magnetic mineral deposits, which can be economically significant as ore bodies (Zhou et al., 2005). For instance, magnetite deposits are found within mafic intrusions along the fault planes in Egypt, which exhibit high magnetic anomalies, facilitating their detection and delineation (Kharbish et al., 2022; Mousa et al., 2020).

606 Also, in Central Iran, iron-bearing magnetic mineral deposits are observed to exhibit high magnetic  
607 and gravity anomalies (Kheyrollahi et al., 2021).

608  
609 Based on current geochemistry data, the Rangpur Saddle holds significant potential for magnetic  
610 mineral ore deposits, driven by its mafic-ultramafic sequences and iron-rich dykes (Ameen et al.,  
611 2021). High  $Fe_2O_3$  content in hornblendites and associated minerals like magnetite and ilmenite  
612 indicate strong magnetization. The tectonic setting, with extensive magmatic intrusions, provides  
613 ideal conditions for mineralization. These findings highlight the region as a possible target for  
614 future geophysical exploration of magnetic ore bodies.



615  
616  
617 Figure 8: 3D schematic diagram illustrating the tectonic structures in Pirganj, where the highest magnetic anomaly is  
618 observed in Bangladesh. The felsic basement, depicted in blue blocks, includes two horsts, as shown in Figure 5d.  
619 Possible mafic intrusions along the faults are indicated in red. Sedimentary layers are represented by a single horizontal  
620 layer in specific colors, with the graben basin likely filled with Gondwana sediments shown in green, and other  
621 sedimentary layers, including alluvium, shown in yellow, which also represents the topography of the region. The  
622 approximate locations of the three drilling logs used in this study (refer to Figure 1b for their locations) are also  
623 indicated.

### 624 625 **5.3 Limitations and Future Research**

626  
627 Compared to other regions globally, limited published research exists for our study area, restricting  
628 our ability to draw on established models and findings. Situated at the eastern edge of the Indian  
629 Shield, this area transitions into a different tectonic subdivision, creating a tectonic complexity  
630 that cannot be fully resolved with the available low-resolution data. The scarcity of high-resolution  
631 datasets, such as regional-scale seismic surveys, further limits our capacity to delineate regional  
632 structures accurately. Currently, no regional or localized high-resolution datasets from ground-  
633 based surveys are widely available, though such data could enhance future studies. Additionally,  
634 the available well log data are predominantly shallow, reaching depths of approximately 500  
635 meters, which limits insights into deeper geological and tectonic features beyond 2 kilometers.  
636 Petrographic descriptions of the basement rocks are also rudimentary, as they are primarily based

637 on a limited number of well logs, most of which were drilled before the 1990s, leaving significant  
638 gaps in our understanding of the area's deeper subsurface geology.

639  
640 Future research in this region will focus on constructing detailed three-dimensional (3D) models  
641 of the subsurface to enhance our understanding of the geological framework. This will involve  
642 compiling a comprehensive dataset repository that integrates historical seismic reflection data,  
643 including those acquired by private entities. Given the shallow nature of the basement, which lies  
644 between approximately 128 and 1000 meters depth, high-resolution gravity and magnetic data will  
645 be critical for resolving fine-scale structural features. To achieve the necessary spatial resolution,  
646 precision ground-based gravity and magnetic surveys are recommended. Specifically, we propose  
647 a targeted geophysical survey in areas exhibiting oval-shaped dipolar magnetic anomalies, using  
648 station spacing of 500 meters or less. Such high-density measurements will improve our ability to  
649 detect and delineate narrow mafic intrusions at shallow depths. In addition, developing a regional  
650 tomographic model using either local earthquake data or ambient seismic noise will provide  
651 complementary constraints on subsurface structures and further refine interpretations of the  
652 geological setting.

653  
654 The study area is characterized by complex tectonic structures shaped by a diverse tectonic history.  
655 While the current study has focused on the Rangpur Saddle, future research will expand to cover  
656 the entire northwestern part of Bangladesh, including the Himalayan Foredeep and the Eocene  
657 Hinge region, which represents a Paleocontinental shelf. Such expanded coverage will provide  
658 deeper insights into the tectonic evolution and geological complexity of the area.

## 659 **Conclusion**

660  
661 This study provides a geophysical investigation of the northwestern region of Bangladesh,  
662 revealing its significant potential for mineral resource exploration. The integration of gravity,  
663 magnetic, seismic, and drilling data has allowed us to identify key tectonic features, such as  
664 gabbroic intrusions along extensional faults, some which may host of valuable magnetic mineral  
665 deposits. Despite the limitations in data resolution and coverage, our findings offer important  
666 insights into the region's geological evolution and resource potential. Future work should prioritize  
667 acquiring more detailed geophysical data and expanding drilling campaigns to refine the  
668 understanding of subsurface structures and evaluate the feasibility of mineral extraction. The  
669 Rangpur Saddle, as the shallowest part of the stable platform, emerges as a promising target for  
670 future mineral exploration endeavors.

## 671 **Data availability**

672  
673 All raw data can be provided by the corresponding authors upon request.

## 674 **Author contribution**

675  
676 Mohammad Tawhidur Rahman Tushar was involved in conceptualization, methodology, software,  
677 validation, formal analysis, investigation, resources, data curation, writing – original draft, writing  
678 – review and editing, visualization. Asif Ashraf contributed to conceptualization, methodology,

682 software, validation, formal analysis, investigation, resources, data curation, writing – original  
683 draft, writing – review and editing, and visualization. Md. Mahfuz Alam worked on software  
684 development, validation, and formal analysis. Md Nasif Jamil contributed to writing – review and  
685 editing and visualization. Saba Karim was involved in writing – review and editing and  
686 visualization. Md. Shahjahan contributed to conceptualization, investigation, resources, project  
687 administration, and supervision. Md. Anwar Hossain Bhuiyan was involved in writing – review  
688 and editing, project administration, supervision, and funding acquisition.

689

## 690 **Competing interests**

691

692 The authors declare that they have no conflict of interest.

693

## 694 **Acknowledgment**

695

696 The gravity, magnetic, and seismic data, along with drilling information used in this study, were  
697 graciously provided by the Geological Survey of Bangladesh (GSB), and the authors deeply  
698 appreciate their support and collaboration. The authors also thank Asef Jamil Ajwad for his  
699 assistance with computational facilities during the research. Special acknowledgment is made for  
700 the Oasis Montaj classroom subscription and for the use of Geosoft Oasis Montaj v8.4 for data  
701 processing and modeling. Finally, gratitude is extended to the Department of Geology, University  
702 of Dhaka, for providing access to essential infrastructure and resources.

703

## 704 **Financial support**

705

706 This work was funded by the National Science and Technology Fellowship, awarded by the  
707 Ministry of Science and Technology, Bangladesh.

708

## 709 **References**

710

711 Adebiyi, L. S., Eluwole, A. B., Fajana, A. O., Salawu, N. B., and Saleh, A.: Contrasting structures  
712 of the Southern Benue trough and the contiguous crystalline basement as observed from high-  
713 resolution aeromagnetic data, *Sci Rep*, 13, 21516, <https://doi.org/10.1038/s41598-023-48639-8>,  
714 2023.

715 Ahamed, S., Hossain, D., and Alam, J.: Exploring Basement Surface relationship of north-west  
716 Bengal Basin using satellite images and tectonic modeling,  
717 <https://doi.org/10.48550/ARXIV.2004.02734>, 2020.

718 Akhtar, A.: Mineral resources and their economic significance in national development:  
719 Bangladesh perspective, *SP*, 250, 127–134, <https://doi.org/10.1144/GSL.SP.2005.250.01.12>,  
720 2005.

721 Alam, M.: Geology and depositional history of Cenozoic sediments of the Bengal Basin of  
722 Bangladesh, *Palaeogeography, Palaeoclimatology, Palaeoecology*, 69, 125–139,  
723 [https://doi.org/10.1016/0031-0182\(89\)90159-4](https://doi.org/10.1016/0031-0182(89)90159-4), 1989.

- 724 Alam, M., Alam, M. M., Curray, J. R., Chowdhury, M. L. R., and Gani, M. R.: An overview of  
725 the sedimentary geology of the Bengal Basin in relation to the regional tectonic framework and  
726 basin-fill history, *Sedimentary Geology*, 155, 179–208, [https://doi.org/10.1016/S0037-](https://doi.org/10.1016/S0037-0738(02)00180-X)  
727 0738(02)00180-X, 2003.
- 728 Alken, P., Thébault, E., Beggan, C. D., Amit, H., Aubert, J., Baerenzung, J., Bondar, T. N., Brown,  
729 W. J., Califf, S., Chambodut, A., Chulliat, A., Cox, G. A., Finlay, C. C., Fournier, A., Gillet, N.,  
730 Grayver, A., Hammer, M. D., Holschneider, M., Huder, L., Hulot, G., Jager, T., Kloss, C., Korte,  
731 M., Kuang, W., Kuvshinov, A., Langlais, B., Léger, J.-M., Lesur, V., Livermore, P. W., Lowes, F.  
732 J., Macmillan, S., Magnes, W., Manda, M., Marsal, S., Matzka, J., Metman, M. C., Minami, T.,  
733 Morschhauser, A., Mound, J. E., Nair, M., Nakano, S., Olsen, N., Pavón-Carrasco, F. J., Petrov,  
734 V. G., Ropp, G., Rother, M., Sabaka, T. J., Sanchez, S., Saturnino, D., Schnepf, N. R., Shen, X.,  
735 Stolle, C., Tangborn, A., Tøffner-Clausen, L., Toh, H., Torta, J. M., Varner, J., Vervelidou, F.,  
736 Vigneron, P., Wardinski, I., Wicht, J., Woods, A., Yang, Y., Zeren, Z., and Zhou, B.: International  
737 Geomagnetic Reference Field: the thirteenth generation, *Earth Planets Space*, 73, 49,  
738 <https://doi.org/10.1186/s40623-020-01288-x>, 2021.
- 739 Ameen, S. M. M., Wilde, S. A., Kabir, Md. Z., Akon, E., Chowdhury, K. R., and Khan, Md. S. H.:  
740 Paleoproterozoic granitoids in the basement of Bangladesh: A piece of the Indian shield or an  
741 exotic fragment of the Gondwana jigsaw?, *Gondwana Research*, 12, 380–387,  
742 <https://doi.org/10.1016/j.gr.2007.02.001>, 2007.
- 743 Ameen, S. M. M., Tapu, A.-T., and Hossain, M. S.: Precambrian Basement Rock of Bangladesh  
744 and Its Metallic Minerals, in: *Bangladesh geosciences and resources potential*, CRC Press Books,  
745 25–54, 2021.
- 746 Arkani-Hamed, J.: Differential reduction to the pole: Revisited, *GEOPHYSICS*, 72, L13–L20,  
747 <https://doi.org/10.1190/1.2399370>, 2007.
- 748 Ashraf, A. and Filina, I.: New 2.75-D gravity modeling reveals the low-density nature of  
749 propagator wakes in the Juan de Fuca plate, *Tectonophysics*, 869, 230127,  
750 <https://doi.org/10.1016/j.tecto.2023.230127>, 2023a.
- 751 Ashraf, A. and Filina, I.: Zones of Weakness Within the Juan de Fuca Plate Mapped From the  
752 Integration of Multiple Geophysical Data and Their Relation to Observed Seismicity, *Geochem*  
753 *Geophys Geosyst*, 24, e2023GC010943, <https://doi.org/10.1029/2023GC010943>, 2023b.
- 754 Balogun, O. B., Akereke, O. F., and Nwobodo, A. D.: Understanding the Constraints to the Correct  
755 Application of the Upward Continuation Operation in Gravity Data Processing, *Pure Appl.*  
756 *Geophys.*, 180, 3787–3811, <https://doi.org/10.1007/s00024-023-03348-1>, 2023.
- 757 Blakely, R. J.: *Potential theory in gravity and magnetic applications*, Cambridge university press,  
758 1996.
- 759 Brune, S., Kolawole, F., Olive, J.-A., Stamps, D. S., Buck, W. R., Buiters, S. J. H., Furman, T., and  
760 Shillington, D. J.: Geodynamics of continental rift initiation and evolution, *Nat Rev Earth Environ*,  
761 4, 235–253, <https://doi.org/10.1038/s43017-023-00391-3>, 2023.

- 762 Calvin, P., Ruiz-Martínez, V. C., Villalaín, J. J., Casas-Sainz, A. M., and Moussaid, B.:  
763 Emplacement and Deformation of Mesozoic Gabbros of the High Atlas (Morocco):  
764 Paleomagnetism and Magnetic Fabrics, *Tectonics*, 36, 3012–3037,  
765 <https://doi.org/10.1002/2017TC004578>, 2017.
- 766 Chowdhury, K. R., Hossain, M. S., and Khan, M. S. H. (Eds.): *Bangladesh geosciences and  
767 resources potential*, First edition., CRC Press, Boca Raton, 610 pp., 2022.
- 768 Curray, J. R.: Geological history of the Bengal geosyncline, *Journal of Association of Exploration  
769 Geophysicists*, 12, 209–219, 1991.
- 770 Curray, J. R. and Moore, D. G.: Sedimentary and Tectonic Processes in the Bengal Deep-Sea Fan  
771 and Geosyncline, in: *The Geology of Continental Margins*, edited by: Burk, C. A. and Drake, C.  
772 L., Springer Berlin Heidelberg, Berlin, Heidelberg, 617–627, [https://doi.org/10.1007/978-3-662-  
773 01141-6\\_45](https://doi.org/10.1007/978-3-662-01141-6_45), 1974.
- 774 DeCelles, P. G.: Foreland Basin Systems Revisited: Variations in Response to Tectonic Settings,  
775 in: *Tectonics of Sedimentary Basins*, edited by: Busby, C. and Azor, A., Wiley, 405–426,  
776 <https://doi.org/10.1002/9781444347166.ch20>, 2011.
- 777 Filina, I., Biegert, E. K., Sander, L., Tschirhart, V., Bundalo, N., and Schiek-Stewart, C.: Integrated  
778 imaging: A powerful but undervalued tool, *The Leading Edge*, 38, 720–724,  
779 <https://doi.org/10.1190/tle38090720.1>, 2019.
- 780 Fuller, R. E. and Waters, A. C.: The Nature and Origin of the Horst and Graben Structure of  
781 Southern Oregon, *The Journal of Geology*, 37, 204–238, 1929.
- 782 Hasan, M. M., Monir, A., and Hassan, M.: Evaluating the Energy and Mineral Resources Prospect  
783 and Future Development in Bangladesh: A Review, <https://doi.org/10.2139/ssrn.4484598>, 2023.
- 784 Hendrickson, M. D.: Geologic interpretation of aeromagnetic and chemical data from the Oaks  
785 Belt, Wabigoon subprovince, Minnesota: implications for Au-rich VMS deposit exploration, *Can.  
786 J. Earth Sci.*, 53, 176–188, <https://doi.org/10.1139/cjes-2015-0141>, 2016.
- 787 Hildenbrand, T. G.: Regional Crustal Structures and Their Relationship to the Distribution of Ore  
788 Deposits in the Western United States, Based on Magnetic and Gravity Data, *Economic Geology*,  
789 95, 1583–1603, <https://doi.org/10.2113/95.8.1583>, 2000.
- 790 Hossain, I., Tsunogae, T., Rajesh, H. M., Chen, B., and Arakawa, Y.: Palaeoproterozoic U–Pb  
791 SHRIMP zircon age from basement rocks in Bangladesh: A possible remnant of the Columbia  
792 supercontinent, *Comptes Rendus Geoscience*, 339, 979–986,  
793 <https://doi.org/10.1016/j.crte.2007.09.014>, 2007.
- 794 Hossain, Md. S., Khan, Md. S. H., Chowdhury, K. R., and Abdullah, R.: Synthesis of the Tectonic  
795 and Structural Elements of the Bengal Basin and Its Surroundings, in: *Tectonics and Structural  
796 Geology: Indian Context*, edited by: Mukherjee, S., Springer International Publishing, Cham, 135–  
797 218, [https://doi.org/10.1007/978-3-319-99341-6\\_6](https://doi.org/10.1007/978-3-319-99341-6_6), 2019.

798 Ibraheem, I. M., Tezkan, B., Ghazala, H., and Othman, A. A.: A New Edge Enhancement Filter  
799 for the Interpretation of Magnetic Field Data, *Pure Appl. Geophys.*, 180, 2223–2240,  
800 <https://doi.org/10.1007/s00024-023-03249-3>, 2023.

801 Jaffal, M., Goumi, N. E., Kchikach, A., Aïfa, T., Khattach, D., and Manar, A.: Gravity and  
802 magnetic investigations in the Haouz basin, Morocco. Interpretation and mining implications,  
803 *Journal of African Earth Sciences*, 58, 331–340, <https://doi.org/10.1016/j.jafrearsci.2010.03.012>,  
804 2010.

805 Jain, A. K., Banerjee, D. M., and Kale, V. S.: *Tectonics of the Indian Subcontinent*, Springer  
806 International Publishing, Cham, <https://doi.org/10.1007/978-3-030-42845-7>, 2020.

807 Kabir, Z. M., Chowdhury, K. R., Akon, E., Kazi, A. I., and Ameen, S. M. M.: Petrogenetic Study  
808 of Precambrian Basement Rocks from Maddhapara, Dinajpur, Bangladesh, *Bangladesh*  
809 *Geoscience Journal*, 7, 1–18, 2001.

810 Khan, A. A. and Rahman, T.: An analysis of the gravity field and tectonic evaluation of the  
811 northwestern part of Bangladesh, *Tectonophysics*, 206, 351–364, [https://doi.org/10.1016/0040-](https://doi.org/10.1016/0040-1951(92)90386-K)  
812 [1951\(92\)90386-K](https://doi.org/10.1016/0040-1951(92)90386-K), 1992.

813 Khan, F. H.: *Geology of Bangladesh*, 1991.

814 Kharbish, S., Eldosouky, A. M., and Amer, O.: Integrating mineralogy, geochemistry and  
815 aeromagnetic data for detecting Fe–Ti ore deposits bearing layered mafic intrusion, Akab El-  
816 Negum, Eastern Desert, Egypt, *Sci Rep*, 12, 15474, <https://doi.org/10.1038/s41598-022-19760-x>,  
817 2022.

818 Kheyrollahi, H., Alinia, F., and Ghods, A.: Regional magnetic and gravity structures and  
819 distribution of mineral deposits in Central Iran: Implications for mineral exploration, *Journal of*  
820 *Asian Earth Sciences*, 217, 104828, <https://doi.org/10.1016/j.jseaes.2021.104828>, 2021.

821 Ma, G., Huang, D., and Liu, C.: Step-Edge Detection Filters for the Interpretation of Potential  
822 Field Data, *Pure Appl. Geophys.*, 173, 795–803, <https://doi.org/10.1007/s00024-015-1053-6>,  
823 2016.

824 Magee, C., Ernst, R. E., Muirhead, J., Phillips, T., and Jackson, C. A.: Magma transport pathways  
825 in large igneous provinces: lessons from combining field observations and seismic reflection data,  
826 in: *Dyke Swarms of the World: A Modern Perspective*, 45–85, 2019.

827 Masum, M., Hoque, M. N., Akbar, M. A., Mahmud, Z., Rana, M. S., Razzaque, M. A., and Amin,  
828 M. A.: Geology and Precambrian Banded Iron Formation formed at Rangpur Platform in  
829 Bangladesh, *International Journal Of Engineering Research And Development*, 17, 43–57, 2021.

830 McCafferty, A. E., Stoesser, D. B., and Van Gosen, B. S.: Geophysical interpretation of U, Th, and  
831 rare earth element mineralization of the Bokan Mountain peralkaline granite complex, Prince of  
832 Wales Island, southeast Alaska, *Interpretation*, 2, SJ47–SJ63, [https://doi.org/10.1190/INT-2014-](https://doi.org/10.1190/INT-2014-0010.1)  
833 [0010.1](https://doi.org/10.1190/INT-2014-0010.1), 2014.

834 Mohamed, A., Abdelrady, M., Alshehri, F., Mohammed, M. A., and Abdelrady, A.: Detection of  
835 Mineralization Zones Using Aeromagnetic Data, *Applied Sciences*, 12, 9078,  
836 <https://doi.org/10.3390/app12189078>, 2022.

837 Moon, J. W.: *The Mineral Industry of Bangladesh*, U.S. Geological Survey, 2022.

838 Morgan, J. P. and McIntire, W. G.: Quaternary Geology of The Bengal Basin, East Pakistan And  
839 India, *Geol Soc America Bull*, 70, 319, [https://doi.org/10.1130/0016-7606\(1959\)70\[319:QGOTBB\]2.0.CO;2](https://doi.org/10.1130/0016-7606(1959)70[319:QGOTBB]2.0.CO;2), 1959.

841 Mousa, S. A. W., Abdel Nabi, S. H., Araffa, S. A. S., Mansour, S. A., and Al Deep, M. A. I.:  
842 Geophysical exploration of titanomagnetite ore deposits by geomagnetic and geoelectric methods,  
843 *SN Appl. Sci.*, 2, 444, <https://doi.org/10.1007/s42452-020-2206-5>, 2020.

844 Mukhopadhyay, D. and Matin, A.: Recent Studies on the Singhbhum Craton, *PINSA*, 86,  
845 <https://doi.org/10.16943/ptinsa/2020/49788>, 2020.

846 Nabighian, M. N.: The Analytic Signal of Two-Dimensional Magnetic Bodies With Polygonal  
847 Cross-Section: Its Properties And Use For Automated Anomaly Interpretation, *Geophysics*, 37,  
848 507–517, <https://doi.org/10.1190/1.1440276>, 1972.

849 Nasuti, Y., Nasuti, A., and Moghadas, D.: STDR: A Novel Approach for Enhancing and Edge  
850 Detection of Potential Field Data, *Pure Appl. Geophys.*, 176, 827–841,  
851 <https://doi.org/10.1007/s00024-018-2016-5>, 2019.

852 Núñez-Demarco, P., Bonilla, A., Sánchez-Bettucci, L., and Prezzi, C.: Potential-Field Filters for  
853 Gravity and Magnetic Interpretation: A Review, *Surv Geophys*, 44, 603–664,  
854 <https://doi.org/10.1007/s10712-022-09752-x>, 2023.

855 Ogah, A. J. and Abubakar, F.: Solid mineral potential evaluation using integrated aeromagnetic  
856 and aeroradiometric datasets, *Sci Rep*, 14, 1637, <https://doi.org/10.1038/s41598-024-52270-6>,  
857 2024.

858 Pham, L. T. and Oliveira, S. P.: Edge Enhancement of Magnetic Sources Using the Tilt Angle and  
859 Derivatives of Directional Analytic Signals, *Pure Appl. Geophys.*, 180, 4175–4189,  
860 <https://doi.org/10.1007/s00024-023-03375-y>, 2023.

861 Pirajno, F. and Santosh, M.: Rifting, intraplate magmatism, mineral systems and mantle dynamics  
862 in central-east Eurasia: An overview, *Ore Geology Reviews*, 63, 265–295,  
863 <https://doi.org/10.1016/j.oregeorev.2014.05.014>, 2014.

864 Rahman, Md. M. and Ullah, S. E.: Inversion of Gravity Data for Imaging of a Sediment-basement  
865 Interface: A Case Study in the Northwestern Part of Bangladesh, *Pure Appl. Geophys.*, 166, 2007–  
866 2019, <https://doi.org/10.1007/s00024-009-0530-1>, 2009.

867 Rangin, C. and Sibuet, J. C.: Structure of the northern Bay of Bengal offshore Bangladesh:  
868 Evidences from new multi-channel seismic data, *Marine and Petroleum Geology*, 84, 64–75,  
869 <https://doi.org/10.1016/j.marpetgeo.2017.03.020>, 2017.

- 870 Reimann, K. U. and Hiller, K.: Geology of Bangladesh, 1993.
- 871 Roest, W. R. and Pilkington, M.: Identifying remanent magnetization effects in magnetic data,  
872 GEOPHYSICS, 58, 653–659, <https://doi.org/10.1190/1.1443449>, 1993.
- 873 Roy, A. B. and Chatterjee, A.: Tectonic framework and evolutionary history of the Bengal Basin  
874 in the Indian subcontinent, *Current Science*, 109, 271–279, 2015.
- 875 Gani, Royhan and Alam, Mustafa: Sedimentation and basin-fill history of the Neogene clastic  
876 succession exposed in the southeastern fold belt of the Bengal Basin, Bangladesh: a high-  
877 resolution sequence stratigraphic approach, *Sedimentary Geology*, 155, 227–270,  
878 [https://doi.org/10.1016/S0037-0738\(02\)00182-3](https://doi.org/10.1016/S0037-0738(02)00182-3), 2003.
- 879 Ruppel, C.: Extensional processes in continental lithosphere, *J. Geophys. Res.*, 100, 24187–24215,  
880 <https://doi.org/10.1029/95JB02955>, 1995.
- 881 Smith, W. H. F. and Sandwell, D. T.: Global Sea Floor Topography from Satellite Altimetry and  
882 Ship Depth Soundings, *Science*, 277, 1956–1962, <https://doi.org/10.1126/science.277.5334.1956>,  
883 1997.
- 884 Sundararajan, N.: A General Perspective on Geophysical Methods in Mineral Exploration, in: On  
885 a Sustainable Future of the Earth's Natural Resources, 53–83, 2012.
- 886 Troll, V. R., Mattsson, T., Upton, B. G. J., Emeleus, C. H., Donaldson, C. H., Meyer, R., Weis, F.,  
887 Dahrén, B., and Heimdal, T. H.: Fault-Controlled Magma Ascent Recorded in the Central Series  
888 of the Rum Layered Intrusion, NW Scotland, *Journal of Petrology*, 61, ega093,  
889 <https://doi.org/10.1093/petrology/egaa093>, 2021.
- 890 Uddin, A. and Lundberg, N.: Unroofing history of the eastern Himalaya and the Indo-Burman  
891 ranges; heavy-mineral study of Cenozoic sediments from the Bengal Basin, Bangladesh, *Journal*  
892 *of Sedimentary Research*, 68, 465–472, <https://doi.org/10.2110/jsr.68.465>, 1998.
- 893 Valdiya, K. S.: *The Making of India*, Springer International Publishing, Cham,  
894 <https://doi.org/10.1007/978-3-319-25029-8>, 2016.
- 895 Veevers, J. J.: Gondwanaland from 650–500 Ma assembly through 320 Ma merger in Pangea to  
896 185–100 Ma breakup: supercontinental tectonics via stratigraphy and radiometric dating, *Earth-*  
897 *Science Reviews*, 68, 1–132, <https://doi.org/10.1016/j.earscirev.2004.05.002>, 2004.
- 898 Zhang, H., Greco, F., Sacek, V., Geng, M., and Liu, P.: Editorial: Applications of gravity  
899 anomalies in geophysics, *Front. Earth Sci.*, 12, 1349161,  
900 <https://doi.org/10.3389/feart.2024.1349161>, 2024.
- 901 Zhang, S., Li, Z.-X., Evans, D. A. D., Wu, H., Li, H., and Dong, J.: Pre-Rodinia supercontinent  
902 Nuna shaping up: A global synthesis with new paleomagnetic results from North China, *Earth and*  
903 *Planetary Science Letters*, 353–354, 145–155, <https://doi.org/10.1016/j.epsl.2012.07.034>, 2012.

904 Zhou, M.-F., Robinson, P. T., Leshner, C. M., Keays, R. R., Zhang, C.-J., and Malpas, J.:  
905 Geochemistry, Petrogenesis and Metallogenesis of the Panzhihua Gabbroic Layered Intrusion and  
906 Associated Fe–Ti–V Oxide Deposits, Sichuan Province, SW China, *Journal of Petrology*, 46,  
907 2253–2280, <https://doi.org/10.1093/petrology/egi054>, 2005.

908